06

Formation of microstructures by non-contact aerosol printing with nanoparticles

© V.V. Ivanov,[1] A.A. Efimov,[1] V.I. Borisov,[1] M.N. Urazov,[1] D.V. Korniushin,[1]
A.G. Musaev,[1] V.A. Voroshilova,[1] V.A. Dolgov,[1] N.P. Simonenko,[2] M.S. Ivanov[1]

[1]Moscow Institute of Physics and Technology, Functional Materials Testing Center,
141701 Dolgoprudny, Moscow region, Russia
[2]Kurnakov Institute of General and Inorganic Chemistry of the Russian Academy of Sciences,
Laboratory of Physical Chemistry of Ceramic Materials,
119991 Moscow, Russia
e-mail: ivanov.vv@mipt.ru

Received April 29, 2025
Revised April 29, 2025
Accepted April 29, 2025

The conditions of aerodynamic focusing of aerosol flows compressed by a flow of focusing gas are analyzed under conditions of contactless aerosol printing with dry metal nanoparticles and microsized ink drops to form small-width lines on substrates. Numerical estimates show that in the processes of movement to the substrate after exiting the nozzle of spherical metal nanoparticles with average sizes more than 70 nm, the Stokes numbers are sufficiently high and the deviations of their trajectories from the flow axis are less than 1 μm, which confirms the possibility of using aerodynamic focusing for printing with dry nanoparticles. Aerosol printing of dry quasi-spherical Au nanoparticles produced arrays in the form of lines with a width of about 30 μm, which demonstrated high plasmon enhancement of the Raman spectrum of low concentrations of the BPE (1,2-bis(4-pyridyl)ethylene) dye of more than $2 \cdot 10^4$. Aerosol printing of quasi-spherical Ag nanoparticles with simultaneous laser sintering made it possible to form monolithic highly conductive microstructures with a sufficiently low specific resistance, exceeding the specific resistance of coarse-crystalline silver by only 2.2 times.

Keywords: Aerosol printing, aerodynamic focusing, metal nanoparticles, plasmon enhancement, highly conductive microstructures.

DOI: 10.61011/TP.2025.09.61929.76-25

Introduction

Among non-contact methods of direct printing of microstructures, which are used in the industry for controllable application of various elements to carrying surfaces according to a programmable figure without application of lithography, the aerosol ink printing that was developed in USA in 2006 is the most promising due to formation of three-dimensional functional elements with a minimum lateral size of up to 10 μm both on flat and relief substrates [1]. The method is based on controllable substrate deposition of focused beams of micro-drops of the ink that are characterized by viscosity within the wide range from 0.5 to 2500 cP. Operability of the ink based on nanomaterials of various chemical compositions, sizes and forms (nanoparticles, nanowires, carbon nanotubes, etc.) as well as high flexibility in creating structures with defined properties allow considering the aerosol printing as a promising trend for creating new elements and devices [2]. Aerosol printers are designed to form 3*D*-interconnections of electron components, transistors on any substrates [3], flexible displays [4], multi-layer ceramic capacitors [5], biological sensors [6] and other elements. Further improvement of economic efficiency of the aerosol ink printing method is fundamentally limited by presence of several necessary additional processes realized before the printing process (synthesis of the nanoparticles and preparing an ink from them) and the microstructure printing process (drying, thermal post-processing).

In 2017, MIPT proposed a new approach of dry aerosol printing without application of ink, which was based on using an aerosol flow of nanoparticles that are synthesized in a repetitively-pulsed spark discharge in the carrying gas between electrodes made of a required consumable material [7]. When using an aerodynamic focusing system of the ink printer, the flow of such Ag and Au nanoparticles was compressed to the diameter of about 100 μm, which allowed printing lines of a respective width on the substrates. It was shown by studies of laser radiation sintering of lines pre-printed by the nanoparticles that this method could form conductive elements on various substrates, in particular, on plastic substrates, in case of sintering by pulsed laser radiation of nanosecond duration [8]. At the same time, aerodynamic focusing did not allow obtaining the line width that is significantly less than 100 μm, which is assumingly related to a morphology of aerosol nanoparticles, which are branched agglomerates. Actually, the primary nanoparticles produced in the area of the pulsed spark discharge have an average size of about 10 nm, while leaving a hot zone of the discharge chamber change and being transported by the

carrying gas to the focusing chamber they are combined into low-density agglomerates with the sizes 100–300 nm [9,10]. These agglomerates are characterized by dominance of a flow resistance force (the Stokes force) over their inertia, which can result in significant widening of the aerosol flow when moving to the substrate during printing [11].

Another drawback of nanoparticle agglomerate printing is a low density of their packaging in the formed array (at most 30 %), which is not sufficient for ensuring complete shrinkage during sintering in order to produce a monolithic solid body [12]. The study [13] has proposed a solution for transforming the nanoparticle agglomerates in the gas flow into solitary nanoparticles of a quasi-spherical form with the sizes from 30 to 120 nm under effect of the nanosecond pulsed laser radiation. In order to provide maximum energy efficiency of transformation of the nanoparticle agglomerates in the gas flow into the solitary nanoparticles of the quasi-spherical form, a method of optimizing values of the parameters of pulsed laser radiation was developed [14]. Embedding a respective optimizing device into the aerosol printer upstream of the aerodynamic focusing system shall simultaneously solve both the problems: to significantly improve focusing of the nanoparticle flow and to increase their packaging density in the formed arrays. The dry aerosol printing printer designed using previous developments combines in a single device four simultaneous processes to be sequentially transmitted by the nanoparticle flow: producing the nanoparticles in the repetitively-pulsed spark discharge, transforming the nanoparticle agglomerates in the gas flow into the solitary nanoparticles of the quasi-spherical form under effect of laser radiation, printing by the aerodynamically-focused nanoparticle flow and laser sintering of the nanoparticle deposited on the substrate.

The present study analyzes conditions of aerodynamic focusing of the flows of quasi-spherical nanoparticles of some metals with the average sizes of about 100 nm and carries out an estimate for forming the lines of a quite small width on the substrates by the dry aerosol printing printer as compared to the ink printing printer. The obtained estimates are confirmed by aerosol printer's formation of the arrays of the quasi-spherical Au nanoparticles in the form of the lines of the width of about 30 μm on the substrates, for which plasmon enhancement of the Raman scattering spectra is studied when determining small concentrations of a test dye. It is investigated whether aerosol printing by the quasi-spherical Ag nanoparticles with simultaneous laser sintering can produce the monolithic highly conductive microstructure with quite low resistivity.

1. Modes of aerodynamic focusing of the flows of the spherical particles

The aerosol printing of the low-width lines on the substrate is provided by two basic effects of the aerosol mechanics: by compressing the aerosol flow by effect of a flow of the focusing (enclosing) gas and providing defined rectilinear motion of the aerosol particles (or drops) from a nozzle exit to the substrate. The aerosol flow is compressed inside the focusing system, whose principal diagram is shown in Fig. 1. The flow of the carrying gas with the aerosol particles is supplied along a central channel into a transition area, where it is cylindrically enveloped with the flow of the focusing gas. Then, the aerosol flow in a shell of the focusing gas is accelerated along the channel of the printing nozzle with a slowly decreasing cross-section towards the nozzle exit. In a correctly designed focusing system, the flows of the aerosol and the focusing gas at subsonic speeds are laminar and axially-symmetrical, thereby preventing their mixing. The Stokes number for the particles in the transition area and the flow velocity are small, but they are great at the exit of the printing nozzle. At the same time, the local flow velocity shall not approximate to the speed of sound to prevent transition of a gas flow into a turbulent mode. The shell of the focusing gas also acts to prevent an impact and deposition of the aerosol particles to the internal wall of the nozzle and to direct the aerosol flow. By increasing the flowrate of the focusing gas Q_s at a fixed value of the aerosol flowrate Q_a, it is possible to additionally decrease a aerosol jet diameter $2R_a$. Thus, a thinly-focused aerosol jet is formed at the nozzle exit, whose diameter can be less than the output nozzle diameter $2R_n$ in several times.

For the laminar mode of flow of the aerosol jet and the focusing gas, which is described by a Poiseuille law, the study [15] has obtained the expression

$$\psi = \sqrt{1 - \frac{\chi}{\chi - 1}}, \qquad (1)$$

which specifies an unambiguous relation of a ratio of the aerosol jet radius and the output nozzle radius $\psi = R_a/R_n$

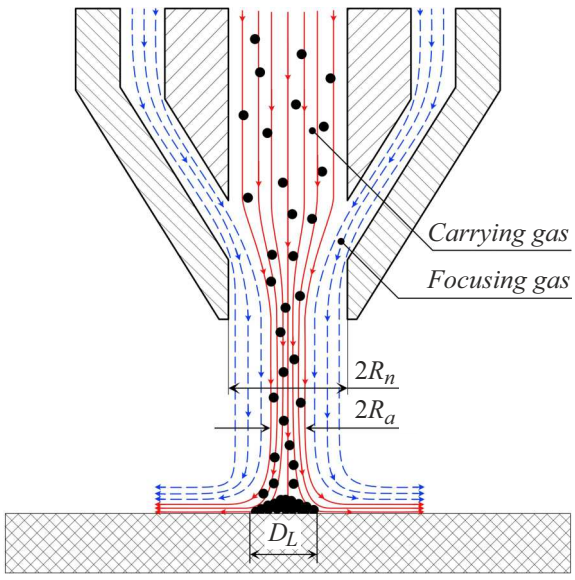

Figure 1. Principle diagram of the focusing system of the aerosol printer.

to a ratio of the flowrates of the focusing gas and the aerosol $\chi = Q_s/Q_a$. For $\chi = 1$ the aerosol jet radius is about a half of the output nozzle radius. It is clear from the dependence (1) that with increase of χ to about 6 a value of ψ quickly decreases, while at high values of χ the decrease of ψ is decelerated with a saturation attainment tend. In particular, when $\chi = 6$, the aerosol jet radius is about in four times less than the output nozzle radius. It is this compression of the aerosol jet that is assumed to be the most effective and is often used in aerosol printing.

The relationship (1) determines the aerosol jet diameter only directly at the nozzle exit, therefore, the width of the printing lines can be identical to the aerosol jet diameter only when the substrate is placed directly at the nozzle exit. With a distance of the substrate from the output nozzle section, the width of the printing lines D_L can be widened due to a number of reasons, the main one of them is deviation of trajectories of the particles (or drops) from a symmetry axis of the focusing system under effect of a perpendicular component of the carrying gas flow, which occurs as a result of collision with the substrate. A degree of deviation of the trajectory of the particles from the system axis is determined by a relationship of a kinetic impulse and a friction force impulse (the Stokes force) of the surrounding viscous gas, which is expressed through the dimensionless Stokes number

$$St = C_m \frac{\rho_p d_p^2 v_g}{9\eta R_a}, \tag{2}$$

where ρ_p — the density of the particle, v_g — the flow velocity of the carrying gas at the nozzle exit η — the dynamic viscosity of the gas, R_a — the aerosol flow radius at the nozzle exit, d_p — the diameter of the particle, C_m — the Cunningham coefficient.

If the Stokes number is much less than unity, then the particles or drops will ideally follow the gas flow line, whereas for the Stokes numbers exceeding unity, the inertia of the particles prevails and they reach the substrate with a minimum deviation of the trajectory. The Stokes number can be regarded as a measure of how easily or not easily the particle moves through a gas medium, in a dependence on its size and density, viscosity and flow velocity of the gas as well as the aerosol jet radius.

For the typical conditions of ink and dry aerosol printing, Table provides estimates of the Stokes numbers St and deviations of the particles trajectory from rectilinear motion to the substrate Δx, which are carried out under a condition of the laminar flow of the gas and the recommended maximum velocity of the aerosol flow in an output narrowing of the nozzle, which is equal to 1/2 of the speed of sound for argon as the carrying gas $v_g = 160.5$ m/s. A degree of compression of the aerosol jet ψ at the output nozzle diameter of 100 μm is assumed to be 0.25, which corresponds to the aerosol flow radius at the nozzle exit $R_a = 12.5\,\mu$m. For the aerosol ink printer, the typical value of the Stokes number when using argon as the carrying gas (dynamic viscosity of $\eta = 22.5\,\mu$Pa·s) for the drops with the average diameter of 1 μm, the density of 1.3 g/cm^3, is about 86, which complies with the data previously obtained in the study [15].

The deviation of the particle trajectory from rectilinear motion to the substrate can be evaluated by an effect of the transverse Stokes force that occurs when rotating the carrying-gas flow near the substrate by 90°. It is directed perpendicular to the original particle trajectory (along the gas flow lines) and determined by the expression

$$F_x = 3\pi\eta d_p v_g. \tag{3}$$

It is assumed for the estimate that the transverse Stokes force acts on the particle during the period of overcoming the carrying-gas flow spreading along the substrate, whence the force action time is $t \approx R_a/v_g$. At the same time, the flow velocity and the layer thickness are equal to the velocity of the aerosol flow and its radius at the nozzle exit, respectively. At the same time, the transverse deviation of the particles when approaching the substrate is evaluated as $\Delta x = a_x t^2/2$, where a_x is a particle acceleration under effect of the Stokes force. Taking into account (3), the estimate of the transverse deviation of the particles is determined by the expression

$$\Delta x \cong \frac{9}{8}\left(\frac{\eta}{\rho_p v_g}\right)\left(\frac{R_a}{d_p}\right)^2. \tag{4}$$

The tabularized calculations according to the expressions (2) and (4) show that when moving to the substrate the spherical metal nanoparticles of the average size of more than 70 nm, while the deviation of their trajectories from the flow axis is below 1 μm (except for aluminum that has the low density). It confirms that it is possible to use aerodynamic focusing both for printing by dry nanoparticles as well as for ink microdrops. We note that during printing by dry nanoparticles with a low mass density additional requirements are imposed on focusing. For example, in order to achieve a quite high value of the Stokes number and small transverse deviation in case of Al, it is required to use the nanoparticles of the diameter of at least 120 nm.

The obtained estimates show that dry aerosol printing by the quasi-spherical nanoparticles using the aerodynamic focusing system is promising for forming the small width of the printing lines that are close to the width of the lines during aerosol ink printing. With the defined sizes of the nanoparticles, the aerodynamic focusing is more effective for the nanoparticles of the metals of the higher density.

2. Dry aerosol printing by the quasi-spherical Au nanoparticles

The dry aerosol printing printer was used to form the arrays of the nanoparticles as the lines on quartz substrates. The nanoparticles were synthesized using the golden high-purity electrodes (99.9999 %). Optimal conditions

Values of the Stokes numbers and transverse deviations of the trajectories for some particles in recommended conditions of aerosol printing

Type particles	Density, g/cm^3	Diameter of particles, nm	Carrying-flow radius at the nozzle exit, μm	Stokes Number	Transverse deviation, μm
Ink microdrops with 30 weight% of Pt nanoparticles	1.3	1000	12.5	85.8	0.02
Pt	21.1	70	12.5	7.32	0.24
Au	19.32	70	12.5	6.70	0.26
Ag	10.5	70	12.5	3.64	0.48
Ni	8.9	70	12.5	3.09	0.57
Al	2.7	70	12.5	0.94	1.86
Al	2.7	120	12.5	2.68	0.63

were selected for sintering the agglomerates into separate nanoparticles of the quasi-spherical form. They were sintered in the gas flow under effect of pulsed laser radiation with the wavelength of 1053 nm (the laser TECH-1053) at the following parameters: the pulse duration of 40 ns, the pulse repetition rate of 500 Hz and the pulse energy of 12 mJ/cm^2. The structures of the small width were formed by arranging the focusing nozzle with the output opening diameter of 100 μm. The size distribution of the produced nanoparticles of the quasi-spherical form, which is recorded in the flow at the nozzle exit by means of the analyzer TSI Inc. MPS 3936 by differential electric mobility, is quite accurately approximated by a lognormal function with the maximums around 120 nm (Fig. 2, *a*). Fig. 2, *b* shows a typical plan-view image of the printed line, which is obtained in the scanning electron microscopy JEOL JSM 7001F to demonstrate even edges of the line at the width of about 30 μm.

We have produced a set of the samples of the printed lines of a various height within the range from 0.2 to 3.2 μm, which were made up of the Au nanoparticles of the quasi-spherical form and studied as plasmon nanostructures for enhancement of the Raman scattering spectra when determining small concentrations of the BPE test dye(1,2-bis(4-pyridil)ethylene) to be more than $2 \cdot 10^4$. For SERS analysis of the chemical composition of the solutions, these nanostructures made up of the gold nanoparticles are of special interest due to high chemical resistance to effects of atmospheric oxygen and test substances as well as compliance of an area of plasmon resonance of the golden nanoparticles to the wavelength of the widely used lasers of the modern Raman spectrometers (532 nm). For the studies at the said wavelength, it is also important to use the substrate of a material that does not exhibit luminescence or intrinsic Raman scattering in the studied spectrum range, which is well corresponded by quartz glass.

The solutions of the BPE test dye with the various concentration were applied to the produced plasmon nanostructures as a drop of the volume of 1 μl by means of a laboratory dispenser (Thermo Scientific 0.1–10 μl). After the solution was dried up, the BPE Raman spectra were measured in the instrument Thermo Scientific DXR Raman Microscope at the following parameters: the excitation laser radiation wavelength of 532 nm, the laser power of 9 mW, the 10x lens, resolution of 4.7–8.7 cm^{-1}, the slotted aperture of 50 μm, a typical diameter of the illuminated spot is 2.1 μm. Single images are obtained by averaging along 10 frames with exposure of 1 s.

The plasmon-structure enhancement factor (EF) was calculated by a ratio of intensities of the two typical peaks of the BPE Raman spectrum (the maximums at 1603 and 1630 cm^{-1}, Fig. 2, *c*): of the SERS spectrum on the nanoparticles, the concentration of the analyte solution was 10^{-4} mol/l, and of the Raman spectrum (on the substrate without nanoparticles), the concentration of the solution was 10^{-2} mol/l (a limiting detectable one without using the nanoparticles):

$$EF = \frac{1}{n} k_i \sum_{i=1}^{n} \frac{I_{SERS_i}}{I_{Raman_i}}, \tag{5}$$

where $k_i = 15.5$ — the correction coefficient that is experimentally obtained based on increase of the signal intensity when the concentration is increased by two orders from 10^{-4} to 10^{-2} mol/l, $n = 2$ — the number of the peaks to be used for calculating enhancement.

Thus, for the produced plasmon nanostructure made up of the Au nanoparticles to have a height of 0.2 μm, the maximum enhancement factor for the BPE dye (1,2-bis(4-pyridil)ethylene) was $1.9 \cdot 10^3$, thereby providing reduction of the limiting detection concentration from 10^{-3} to 10^{-6} mol/l (Fig. 2, *c*).

For the printed lines made of the Au nanoparticles, which have a various height, the plasmon enhancement profile for the BPE dye was measured by recording the Raman spectra from a serial number of areas across the line with

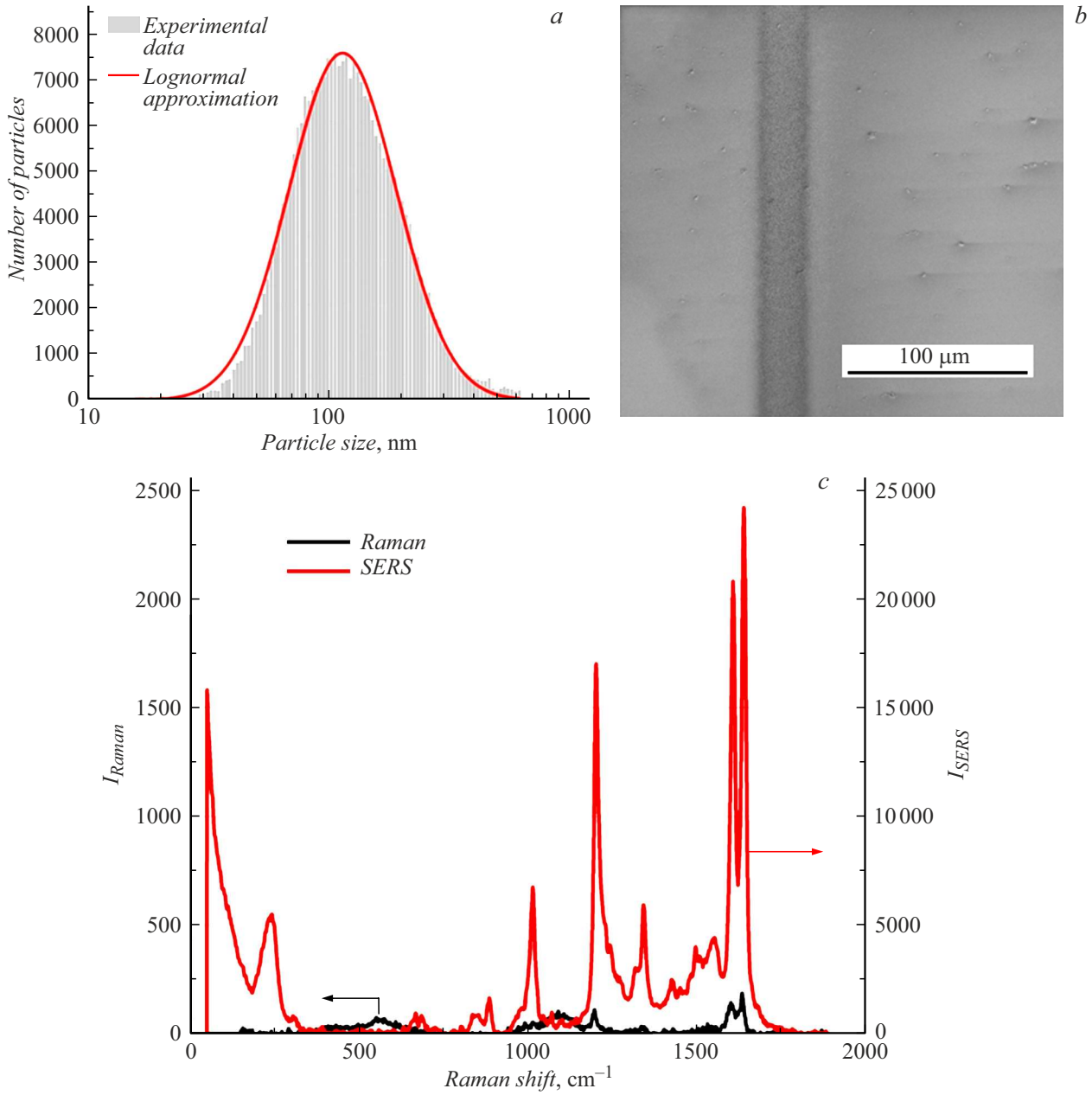

Figure 2. *a* — the size distribution of the Au nanoparticles at the exit of the focusing nozzle; *b* — the SEM image of the plasmon nanostructure as the printing line; *c* — comparison of the BPE spectra (1,2-bis(4-pyridil)ethylene): the red color marks the SERS-spectrum obtained for the solution of the concentration of 10^{-4} mol/l on the printing line of the height of 0.1 μm, while the black color marks the initial Raman spectrum for the solution of the concentration of 10^{-2} mol/l.

a distance of 3 μm between the centers of the adjacent areas in an automated mode. Fig. 3 shows the obtained plasmon enhancement profiles together with a geometrical line profile measured by the optical profilometer Sensofar S-Neox, for the three typical lines of the various height. The dependences of the plasmon enhancement factor for the BPE dye on the local line height are compared to show that the enhancement factor is increased to the line height of about 1.5 μm. The second effect is that there is a local maximum of the plasmon enhancement factor around the maximum of the line profile with the increased heights in the samples (*a*) and (*b*).

The first effect of increase of the plasmon enhancement factor with increase of the line thickness can be logically related to penetration of laser radiation and output of the Raman scattering signal to a certain depth of the array of the nanoparticles, which is about 1.5 μm (about 20 layers of the nanoparticles). The effect of the local minimum of the plasmon enhancement factor around the maximum of the line profile can be explained by joint manifestation of

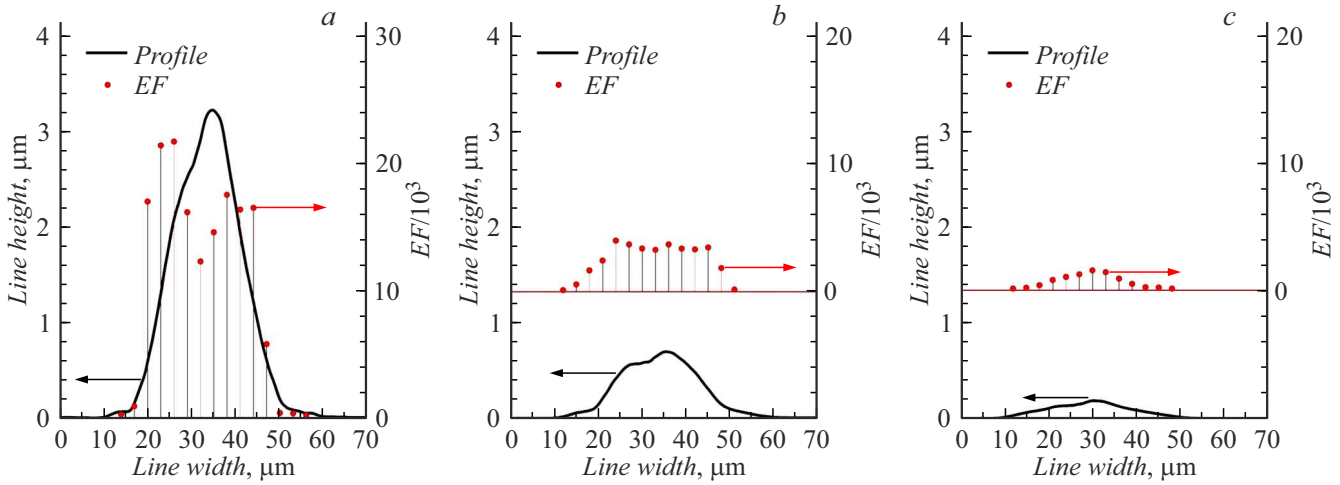

Figure 3. Profiles of the plasmon nanostructures and the values of the plasmon enhancement factor with the printing line thickness of 3.2 (*a*), 0.8 (*b*) and 0.2 μm (*c*).

the two following patterns. First of all, since the spectrum of size distribution of the particles includes a large number of the particles of the small sizes of up to 30 nm and of the big sizes of up to 300 nm (Fig. 2, *a*), then, according to (4), the small-sized particles, when being deposited to the substrates, shall deviate for a larger distance from the aerosol flow center, thereby resulting in deposition of a larger portion of the big particles in the central zone of the formed line and domination of the smaller particles on line slopes. Secondly, it has been previously shown theoretically and experimentally that the golden nanoparticles with the sizes 50–80 nm are characterized by much larger extinction of radiation within the area of plasmon resonance than the larger particles [16]. In this regard, plasmon enhancement can be pronounced more strongly on the slope of the printing trail (Fig. 3), since in this area the average size of the particles has a stronger effect of plasmon resonance for the probing radiation wavelength of 532 nm.

Due to the demonstrated high plasmon enhancement, the plasmon nanostructured produced by dry aerosol printing can be widely applied in surface enhanced Raman-scattering spectroscopy (SERS) both in scientific research as well as in practical medicine, pharmaceutics, forensic science and restoration of art pieces [17]. Besides, large prospects of application of the technology of aerosol printing of the plasmon nanostructures from some metals are expected for improving efficiency of some optoelectronic devices, in particular, solar panels and light-diode emitters [18].

3. Dry aerosol printing of the highly conductive elements by the Ag nanoparticles with simultaneous laser sintering

The conductive structures were printed by the aerosol printer using silver electrodes (of purity of 99.9999 %) in optimized conditions of the gas-discharge synthesis of the nanoparticles and transformation of the nanoparticle agglomerates in the gas flow into the solitary nanoparticles of the quasi-spherical form under effect of repetitively-pulsed laser radiation with characteristics that are given above for forming the golden plasmon nanostructures. At the same time, it used the focusing system with the output nozzle diameter of 200 μm and the repetitively-pulse laser Tech-527 of the radiation wavelength of 527 nm and pulse duration of 20 ns for sintering of the arrays of the nanoparticles when they are deposited on the quartz glass substrates.

High conductivity of the Ag microstructures is achieved by sintering the quasi-spherical nanoparticles, when they are deposited to the substrate, under effect of pulsed laser radiation of the energy density of about 200 J/cm^2. Using laser radiation with the wavelength of 532 nm that is close to a frequency of the maximum of plasmon resonance on the Ag particles (420 nm) provides high efficiency of absorption of the radiation energy by the nanoparticles of the diameter 50–100 nm and combined with nanosecond pulse duration does not induce significant heating of the substrate. Laser radiation is input into the printing chamber through a window using a long-focus lens and a motorized dielectric mirror, which are arranged outside the chamber.

As can be seen from the images of Fig. 4, aerosol printing by the quasi-spherical Ag nanoparticles with simultaneous laser sintering provides high monolithicity of the structure of the array of the nanoparticles with a minimum number of pores. It results in high resistivity of nanostructured silver with the sizes of the crystallites of about 50–100 nm — up to 3.54 mΩ·cm, which is about 220 % of resistivity of large-crystal silver. Resistivity of the sintered silver lines was determined based on data of measurements of absolute resistance of the lines in a four-contact method by the multimeter Fluke 287 and of their cross-sectional profile

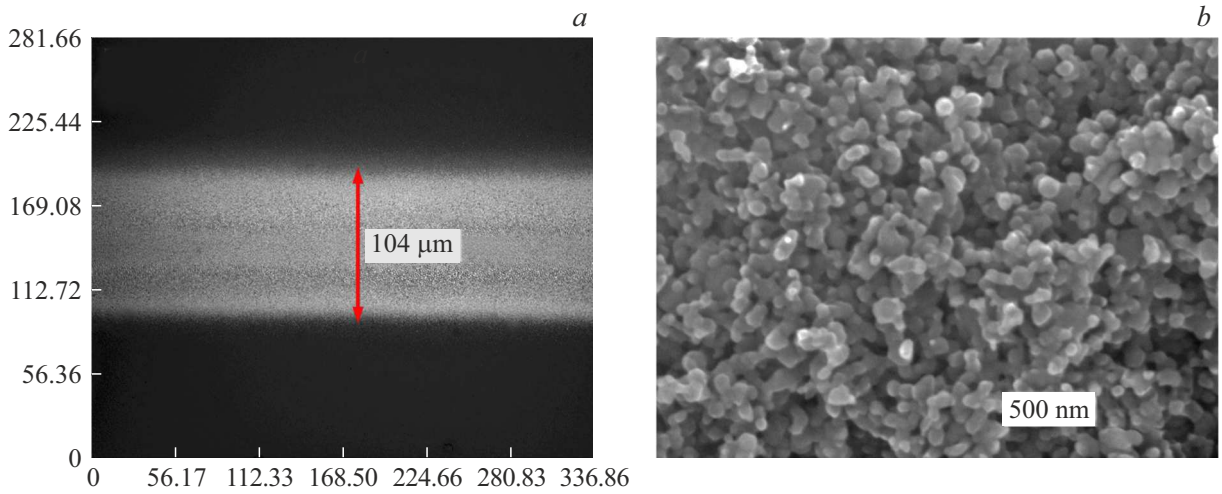

Figure 4. *a* — the plan-view image of the sintered line from the Ag nanoparticles, as obtained in the optical microscope; *b* — the image of a microstructure of a fracture of the sintered line, as obtained in the scanning electron microscope JEOL JSM 7001F.

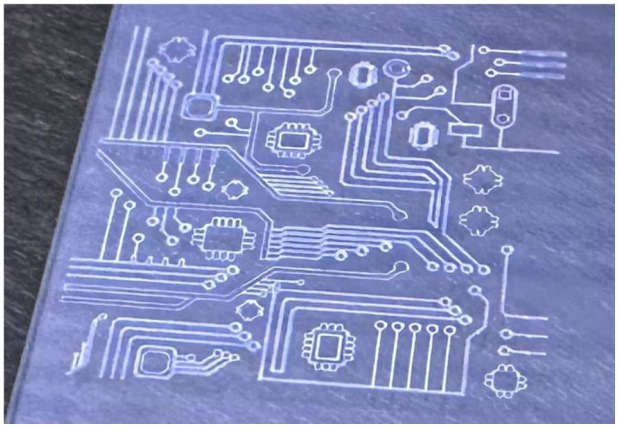

Figure 5. Photo of the wiring mockup of the electronic board.

and length by means of the optical profilometer Sensofar S-Neox.

The obtained value of resistivity for the nanocrystalline silver is close to a limit index, since along with scattering of free electrons on phonons it is also significantly contributed by scattering on intercrystalline boundaries. Actually, the mean free path of an electron in a volume sample of silver is 52 nm [19], which is comparable to the size of the nanocrystals in the samples produced by aerosol printing.

The developed mode of dry aerosol printing was taken with simultaneous laser sintering to manufacture the wiring mockup of the electronic board by silver printing on the quartz glass substrate (Fig. 5). This structure is manufactured in an automated mode as per the given drawing. Since the printing process is realized in the closed vacuumed chamber in a residual inert atmosphere of argon, it is possible to print the microstructures by other metals as well, including copper, nickel, etc.

Conclusion

The processes of aerodynamic focusing of the flows of the quasi-spherical metal nanoparticles have been analyzed to show that at the average sizes of the nanoparticles, which exceed 70 nm, the deviations of their trajectories from the flow axis do not exceed 1 μm, which enables using this approach for printing by the dry nanoparticles. With applying aerosol printing by the dry Au and Ag nanoparticles of the quasi-spherical form, we have implemented formation of the arrays as the lines of the width of up to 30 μm and of quite dense packaging of the nanoparticles. Simultaneous laser sintering of the arrays of the Ag nanoparticles provides formation of the monolithic highly conductive microstructures with quite low resistivity that only in 2.2 times exceeds resistivity of the volume silver.

Funding

This study is supported by the Ministry of Science and Higher Education of the Russian Federation under Agreement № 075-15-2024-560 (13.1902.24.31).

Conflict of interest

The authors declare that they have no conflict of interest.

References

[1] M.J. Renn. USA Patent 7108894B2 (2006)
[2] T. Seifert, M. Baum, F. Roscher, M. Wiemer, T. Gessner. Mater. Today Proc., **2**, 4262 (2015).
[3] C.S. Jones, X. Lu, M. Renn, M. Stroder, W.-Sh. Shih. Microelectron. Eng., **87**, 434 (2010).
[4] C. Yang, E. Zhou, S. Miyanishi, K. Hashimoto, K. Tajima. ACS Appl. Mater. Interfaces, **3**, 4053 (2011).

[5] C.E. Folgar, C. Suchicital, S. Priya. Mater. Lett., **65**, 1302 (2011).
[6] I. Grunwald, E. Groth, I. Wirth, J. Schumacher, M. Maiwald, V. Zoellmer, M. Busse. Biofabrication, **2**, 14106 (2010).
[7] A.A. Efimov, G.N. Potapov, A.V. Nisan, V.V. Ivanov. Results Phys., **7**, 440 (2017).
[8] K. Khabarov, D. Kornyushin, B. Masnaviev, D.N. Tuzhilin, A.A. Efimov, D.L. Saprykin, V.V. Ivanov. Appl. Sci., **10** (1), 246 (2020).
[9] K.E.J. Lehtinen, R.S. Windeler, S.K. Friedlander. J. Aer. Sci., **27**, 883 (1996).
[10] N.S. Tabrizi, M. Ullmann, V.A. Vons, U. Lafont, A. Schmidt-Ott. J. Nanopart. Res., **11**, 315 (2009).
[11] W.C. Hinds. *Aerosol technology: properties, behavior, and measurement of airborne particles*. 2nd eds. (Wiley-Interscience, 1999)
[12] M.J. Mayo. Interna. Mater. Rev., **41** (3), 85 (2013).
[13] K. Khabarov, M. Nouraldeen, S. Tikhonov, A. Lizunova, A. Efimov, V. Ivanov. Nanomaterials, **11**, 2701 (2021).
[14] M.N. Urazov, V.A. Dolgov, M.S. Ivanov, V.V. Ivanov, V.A. Voroshilova, D.V. Kornyushin, V.I. Borisov. Patent RF RU2828069C1. Byul. № 28 (2024) (in Russian).
[15] S. Binder, M. Glatthaar, E. Rädlein. Aer. Sci Tech., **9** (48), 924 (2014).
[16] S.V. Gaponenko, D.V. Guzatov. Pr. IEEE, **108** (5), 704 (2020).
[17] N.Yu. Zhigalov, V.F. Gol'chevskii, I.L. Badzyuk. "Vestnik" MVD Moscow russian university, **2**, 14 (2017).
[18] T.Yu. Mogil'naya, Yu.L. Krit, N.V. Morozova, V.V. Kuvshinov, V.V. Sleptsov, M.V. Fedotikova, L.L. Pagava, M.Yu. Gorozheev. EOM, **6**, 67 (2020) (in Russian).
[19] P.B. Johnson, R.W. Christy. Phys. Rev., **6** (12), 4370 (1972).

Translated by M.Shevelev